

Electronic and Vibrational Spectroscopy and Vibrationally Mediated Photodissociation of $V^+(OCO)$

Murat Citir, Gokhan Altinay, and Ricardo B. Metz*

Department of Chemistry, University of Massachusetts Amherst, Amherst, Massachusetts 01003

Received: January 18, 2006; In Final Form: February 24, 2006

Electronic spectra of gas-phase $V^+(OCO)$ are measured in the near-infrared from 6050 to 7420 cm^{-1} and in the visible from 15 500 to 16 560 cm^{-1} , using photofragment spectroscopy. The near-IR band is complex, with a 107 cm^{-1} progression in the metal–ligand stretch. The visible band shows clearly resolved vibrational progressions in the metal–ligand stretch and rock, and in the OCO bend, as observed by Bruccat and co-workers. A vibrational hot band gives the metal–ligand stretch frequency in the ground electronic state $\nu_3'' = 210 \text{ cm}^{-1}$. The OCO antisymmetric stretch frequency in the ground electronic state (ν_1'') is measured by using vibrationally mediated photodissociation. An IR laser vibrationally excites ions to $\nu_1'' = 1$. Vibrationally excited ions selectively dissociate following absorption of a second, visible photon at the $\nu_1' = 1 \leftarrow \nu_1'' = 1$ transition. Rotational structure in the resulting vibrational action spectrum confirms that $V^+(OCO)$ is linear and gives $\nu_1'' = 2392.0 \text{ cm}^{-1}$. The OCO antisymmetric stretch frequency in the excited electronic state is $\nu_1' = 2368 \text{ cm}^{-1}$. Both show a blue shift from the value in free CO_2 , due to interaction with the metal. Larger blue shifts observed for complexes with fewer ligands agree with trends seen for larger $V^+(OCO)_n$ clusters.

Introduction

Photofragment spectroscopy has been widely used to measure electronic^{1–5} and vibrational^{6–10} spectra of ions. The recent growth in photofragment *vibrational* spectroscopy of ions is due to both philosophical and practical considerations. Vibrational spectroscopy is an outstanding tool to study bonding and can give structural information even in quite complex molecules. Laboratory optical parametric oscillator systems provide tunable infrared light with improved performance in the 2–5 μm region where the vibrations of many molecules lie, while free electron lasers provide high fluences out to $\sim 17 \mu\text{m}$. Photofragment spectroscopy requires that photon absorption lead to dissociation. This poses a challenge for vibrational spectroscopy of small transition metal–ligand complexes, which are often bound by $> 4000 \text{ cm}^{-1}$. Several complementary techniques have been used to circumvent this problem.

IR multiphoton photodissociation (IRMPD) can be achieved by IR radiation with high laser fluences. Photodissociation requires that clusters be excited with sufficient energy to break the weakest bond and that this energy find its way from the coordinate excited to the dissociation coordinate. A high density of vibrational states and efficient intramolecular vibrational redistribution (IVR) facilitate IRMPD by maintaining the resonance that would otherwise be lost due to anharmonicity and by transferring energy from the ligand vibration excited to the dissociation coordinate (usually the metal–ligand stretch). Small clusters are expected to have relatively high binding energies and low IVR rates. With cluster size the density of states increases and this enhances both multiphoton absorption and IVR rates.

The other approach used often in IR photodissociation spectroscopy has been the addition of a weakly bound spectator “tag” atom or molecule, usually a rare gas atom.^{9,11,12} IR

absorption by the ion core leads to vibrational predissociation and loss of the tag. The choice of the tag is a compromise between weak binding to ensure one-photon dissociation and minimize perturbation of the structure and vibrations of the ion core, and sufficiently strong binding to produce useful quantities of tagged ions. Argon is often used as the tag. For small ions, even tagging can give low photofragment signals, as inefficient IVR can lead to a low vibrational predissociation rate.

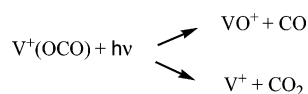
Vibrationally mediated photodissociation (VMP) provides a means to measure the vibrational spectra of small, strongly bound complexes such as $V^+(OCO)$. VMP is a double resonance technique in which the molecule is first vibrationally excited, a second photon then promotes the vibrationally excited molecule to a dissociative electronic state in the ultraviolet or visible region.^{13–15} Successful VMP requires that the vibrationally excited molecules have a different photodissociation spectrum from the vibrationally unexcited molecules. Although VMP is less generally applicable to ion spectroscopy than IRMPD or tagging, it has the potential to obtain unperturbed vibrational spectra, with high spectral resolution. With neutral molecules, VMP experiments usually measure the spectroscopy of regions of the excited-state potential energy surface that are not Franck–Condon accessible from the ground state and show how different vibrations affect the photodissociation dynamics. In this paper, we use VMP to measure the OCO antisymmetric stretch frequency in $V^+(OCO)$.

Industrial processes and the burning of fossil fuels produce large amounts of CO_2 .¹⁶ Recycling CO_2 by converting it to useful compounds is thus an attractive idea that has received much attention.¹⁷ Carbon dioxide is a major component of the water gas shift reaction, which is used to produce high-purity hydrogen.¹⁸ Using vanadium as a dopant improves the efficiency of the iron oxide based water gas shift catalyst.¹⁹

The structures, binding energies, and electronic and vibrational spectroscopy of $V^+(OCO)_n$ complexes have been extensively studied by theory,²⁰ collision-induced dissociation,²¹ and

* Address correspondence to this author. E-mail: rbmetz@chemistry.umass.edu.

photofragment spectroscopy.^{22,23} Bauschlicher and co-workers calculated structures and binding energies of $M^+(\text{OCO})$ complexes for the first-row transition metal cations.²⁰ They found that the linear end-on $M^+-\text{OCO}$ structure is the most favorable electrostatically bound structure. For the early transition metals Sc^+ , Ti^+ , and V^+ , the inserted OM^+-CO structure is more stable. Binding of V^+ (^5D , $3d^4$) to CO_2 leads to $^5\Sigma$, $^5\Pi$, and $^5\Delta$ states of $\text{V}^+(\text{OCO})$, depending on which d-orbital is empty. At the B3LYP level, the ground state is $^5\Delta$ with a V^+-OCO bond length of 2.103 Å and a dissociation energy of 0.99 eV, while the $^5\Sigma$ state is calculated to lie 0.08 eV higher. Calculations at the CCSD(T) level predict a $^5\Sigma$ ground state bound by 0.79 eV, while the $^5\Delta$ state is 0.09 eV higher in energy.²⁰ Experimentally, Armentrout and co-workers used guided ion beam tandem mass spectrometry to measure the bond dissociation energy $D_0(\text{V}^+-\text{CO}_2) = 0.75 \pm 0.04$ eV.²¹ Brucat and co-workers measured the photodissociation spectrum of $\text{V}^+(\text{OCO})$ in the visible.²² The spectrum is vibrationally resolved, and they assigned progressions in the V^+-OCO stretch and rock, and in the OCO bend. Dissociation occurs by two pathways:



Photodissociation is somewhat mode selective, with the branching ratio depending on which vibronic feature is excited.²² Recently, Duncan and co-workers reported a study of $\text{V}^+(\text{OCO})_n$ and $\text{V}^+(\text{OCO})_n\text{Ar}$ cluster ions by infrared resonance enhanced photodissociation spectroscopy.²³ Vibrational resonances were identified and assigned in the region of the antisymmetric stretch of free CO_2 at 2349.16 cm^{-1} . They did not observe photodissociation of $\text{V}^+(\text{OCO})$, and even $\text{V}^+(\text{OCO})_2$ has a low photofragmentation yield. In the argon-tagged complex $\text{V}^+(\text{OCO})\text{Ar}$, they observe a relatively weak band at 2378 cm^{-1} .

The $\text{V}^+(\text{OCO})$ complex is a good candidate for vibrationally mediated photodissociation studies because of the strong IR absorption expected for the OCO antisymmetric stretch vibration and because its electronic absorption spectrum is highly structured. In this paper, we report an experimental study of the electronic and vibrational spectroscopy of $\text{V}^+(\text{OCO})$. A further motivation for the study of $\text{V}^+(\text{OCO})$ is to investigate mode selective dissociation in vibrational bands involving the OCO antisymmetric stretch. Those results will be presented separately.

Experimental Approach

These studies were carried out on a dual time-of-flight reflectron photofragment spectrometer that has been described in detail previously.^{5,24} Vanadium cations are generated by laser ablation of a rotating and translating vanadium rod (Sigma-Aldrich, 99.98% pure). Ablated V^+ interacts with $\sim 0.08\%$ carbon dioxide (UHP grade, 99.98% pure) in helium (UHP grade, 99.98% pure) introduced through a piezoelectric pulsed valve to produce $\text{V}^+(\text{OCO})_n$ ($n \geq 1$). Collisions with the bath gas cool the ions prior to and during expansion into vacuum. These conditions produce electronically and vibrationally cold ions with rotational temperatures of ~ 12 K. Strong $\text{V}^+(\text{OCO})$ signals are also obtained from more concentrated mixtures by adjusting the laser-pulsed valve and valve-extraction timings to favor small clusters. However, these conditions lead to $\text{V}^+(\text{OCO})$ that is noticeably vibrationally and rotationally hotter. The ab initio calculations²⁰ and guided ion beam experiments²¹ clearly show that inserted $\text{OV}^+(\text{CO})$ is more stable than the

linear $\text{V}^+(\text{OCO})$ isomer. However, the guided ion beam experiments also show that although the $\text{V}^+ + \text{CO}_2 \rightarrow \text{VO}^+ + \text{CO}$ reaction is exothermic and has no barrier, it is spin-forbidden and extremely inefficient, occurring in only 1 of every 6000 collisions.²¹ Under our experimental conditions, we likely produce both isomers. On the basis of the spectroscopy and observed product channels, we only photodissociate $\text{V}^+(\text{OCO})$. This observation has also been made by Brucat and co-workers²² and Duncan and co-workers,²³ who used similar ion sources to ours to study the spectroscopy of $\text{V}^+(\text{OCO})_n$ clusters.

Ions produced in the source pass through a skimmer and are extracted along the beam axis by using a pulsed electric field, accelerated to 1800 V kinetic energy, and re-referenced to ground potential prior to entering the field-free flight tube. An Einzel lens and a series of deflectors guide the ions into the detector chamber. A final deflector allows the ion beam to traverse the 5° angle through the reflectron and to the detector. Ions are photodissociated at the turning point of the reflectron with pulsed lasers. Photofragment ions and undissociated parent ions reaccelerate out of the reflectron and impinge upon a 40 mm diameter dual microchannel plate detector. Masses of parent and fragment ions are determined from their flight times.

Photodissociation is effected by one-photon absorption in the near-IR, one-photon absorption in the visible, or visible absorption by vibrationally excited molecules prepared by mid-IR absorption. The visible laser system is a Nd:YAG pumped dye laser with < 0.08 cm^{-1} line width. An IR OPO/OPA (Laser Vision) pumped by another injection-seeded Nd:YAG laser produces light in the near- and mid-infrared. The IR laser system uses a combination of a 532 nm pumped OPO and a 1064 nm pumped OPA. It produces 3–9 mJ/pulse from 6050 to 7425 cm^{-1} in the near-IR. It is also tunable from 2100 to > 4000 cm^{-1} in the mid-IR, producing 3 mJ/pulse near 2400 cm^{-1} , with a 0.2 cm^{-1} line width. The mid-IR and near-IR laser wavelengths are calibrated by using the photoacoustic spectra of methane and water, respectively.²⁵ The dye laser is calibrated by using the absorption spectrum of I_2 .²⁶ For the vibrationally mediated photodissociation experiments, the delay between the IR and visible lasers is ~ 40 ns.

The ion signal is amplified, collected on a digital oscilloscope or a gated integrator, and averaged with a LabView based program. The immediate identification of the dissociation channels at a given wavelength is possible by using a *difference spectrum*, which is generated by subtracting spectra collected with the dissociation laser blocked from those when it is unblocked. The *photodissociation spectrum* of a specific channel is obtained by monitoring the yield of the corresponding fragment ion as a function of wavelength and normalizing to parent ion signal and laser fluence.

Results

Electronic Spectroscopy. Figure 1 shows schematic potential energy surfaces for the ground and several excited quintet states of $\text{V}^+(\text{OCO})$. Transitions from the $\text{V}^+(\text{OCO})$ ground state to the second excited state shown, which correlates to V^+ (^5P , $3d^3-4s$), were observed by Brucat and co-workers²² with the origin at 15 801 cm^{-1} . This will be referred to as the [15.8] state. Transitions to the first excited state shown, which correlates to V^+ (^5F , $3d^34s$), should occur in the near-IR.²⁷ We thus first measured the photodissociation spectrum of $\text{V}^+(\text{OCO})$ starting near the bond dissociation energy of 6050 ± 320 cm^{-1} measured by Armentrout and co-workers using guided ion beam mass spectrometry.²¹ Figure 2 shows the photodissociation spectrum of $\text{V}^+(\text{OCO})$ in the near-IR. At low energy, the photodissocia-

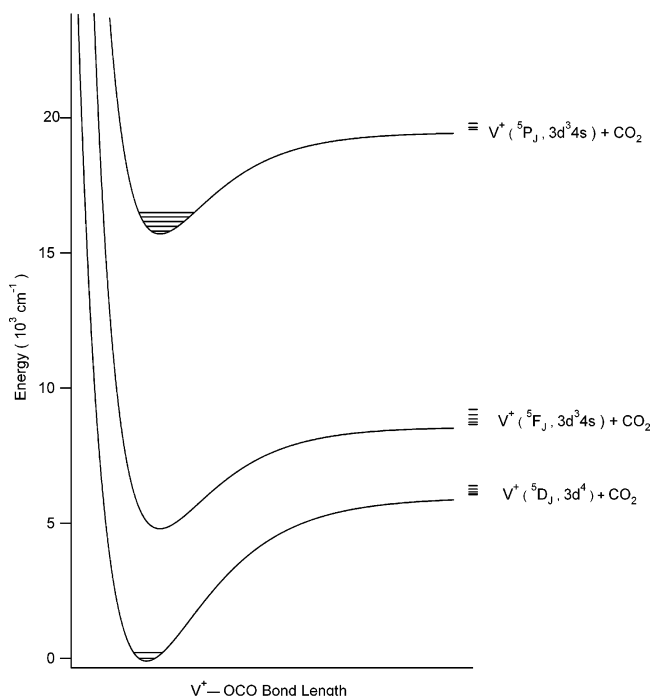


Figure 1. Semiquantitative potentials for several quintet electronic states of $V^+(OCO)$. Energies of states and spin-orbit levels of V^+ are from ref 27. Interaction of $V^+(^3D, 3d^4)$ with CO_2 leads to $^5\Sigma$, $^5\Pi$, and $^5\Delta$ states with very similar energies, depending on which d-orbital is empty. Similar considerations apply to the other states of V^+ . In each case, only one of these states is shown. The V^+-CO_2 binding energy (ref 21) determines the well depth of the $V^+(OCO)$ ground state; the well depth of the excited state correlated to $V^+(^3P)$ is based on its spectroscopy (ref 22 and this work). The bond length and well depth of the state correlating to $V^+(^5F, 3d^3 4s)$ is assumed to be the same as that of the state correlating to $V^+(^5P, 3d^3 4s)$.

tion spectrum is obtained via difference spectra due to low dissociation yield. Loss of CO_2 is the only observed dissociation channel. At higher energies, the dissociation yield increases, and the photodissociation spectrum is obtained by monitoring the yield of V^+ as a function of wavelength and normalizing to the parent ion signal and laser power. The gradual increase in photodissociation near threshold suggests that the observed onset is not due to thermodynamics, but rather is spectroscopic, due to poor Franck-Condon overlap with excited states of $V^+(OCO)$ near threshold. At higher energy, the spectrum has a series of peaks spaced by $\sim 25\text{ cm}^{-1}$, with the pattern repeating after 107 cm^{-1} . The 107 cm^{-1} spacing is assigned as a progression in the V^+-OCO stretch in the excited state, while the 25 cm^{-1} progression is likely the V^+-OCO rock. These results are summarized in Table 1, and this state is referred to as the [6.0] state.

The primary goal of this work is to measure the OCO antisymmetric stretch vibration of $V^+(OCO)$. This can be accomplished by using vibrationally mediated photodissociation (VMP) if vibrationally excited molecules have a different photodissociation spectrum from ground state molecules. Previous VMP studies, on neutral molecules, typically rely on a broad photodissociation spectrum shifting to lower energy following vibrational excitation. In this case, $V^+(OCO)$ has a vibrationally resolved photodissociation spectrum in the visible,²² and we find that vibrational excitation shifts the positions of these sharp peaks.

Figure 3 shows the photodissociation spectrum of $V^+(OCO)$ over the range of $15\,500$ to $16\,530\text{ cm}^{-1}$. The spectrum agrees with the results of Brucat and co-workers,²² who also observe

similar, vibrationally resolved spectra for complexes of V^+ with Ar, Kr, and CH_4 .²⁸⁻³⁰ The assignment of this spectrum places the origin at the reddest peak ($15\,801\text{ cm}^{-1}$), and gives frequencies for several vibrations in the excited state: the V^+-OCO stretching mode $\nu_3' = 186\text{ cm}^{-1}$ ($\omega_e = 196\text{ cm}^{-1}$, $\omega_e x_e = 4.7\text{ cm}^{-1}$),²² the OCO bend $\nu_4' = 597\text{ cm}^{-1}$, and the V^+-OCO rocking motion $\nu_5' = 105\text{ cm}^{-1}$, all in agreement with the earlier study.²² Under appropriate source conditions, we observe a hot band at $15\,591\text{ cm}^{-1}$ that is shifted by 210 cm^{-1} from the origin and is assigned to the V^+-OCO stretch in the ground state, ν_3'' (see Table 1).

Vibrational Spectroscopy and Vibrationally Mediated Photodissociation. We measure the CO_2 antisymmetric stretch frequency in the $V^+(OCO)$ ground state using two techniques. The first one is infrared depletion spectroscopy. This technique was first introduced by Lee and co-workers to study fundamental and overtone vibrations of benzene and its dimer³¹ and has been used by several groups to study neutral clusters and biomolecules.³²⁻³⁶ In IR depletion spectroscopy of neutrals, a UV laser is tuned to a vibronic transition from the ground vibrational state, producing ions by 1+1 REMPI. A tunable IR laser fires before the UV laser. Absorption of infrared photons removes population from the ground state. This is observed as a decrease in the ion signal (hence the technique is often referred to as ion-dip spectroscopy). In this work, we use the same logic with a small modification. A visible laser excites the $\nu_1' = 0 \leftarrow \nu_1'' = 0$ band of $V^+(OCO)$ at $15\,801\text{ cm}^{-1}$, producing fragment ions. An IR laser is tuned in the region of the OCO antisymmetric stretch vibration. On resonance, it excites some molecules to $\nu_1'' = 1$ and we expect to see depletion of the fragment signal. As seen in Figure 4 (top), we observe 8% depletion at 2391.5 cm^{-1} . Each data point is obtained from IR laser on-laser off difference spectra normalized to the area under the IR laser off fragment peak.

This experiment establishes the position of the antisymmetric stretch band and that *at least* 8% of the ions are vibrationally excited. This value is only a lower limit because molecules in the $\nu_1'' = 1$ state may absorb at $15\,801\text{ cm}^{-1}$ and photodissociate. The depletion experiment has a major disadvantage. We are trying to observe a small decrease in the fragment ion signal, which is not particularly large or stable. Obtaining good signal-to-noise thus requires extensive signal averaging, which limits the number of data points we can measure.

To measure the vibrational spectrum using an enhancement experiment, we first find the $\nu_1' = 1 \leftarrow \nu_1'' = 1$ electronic transition. The IR laser is fixed at 2391.5 cm^{-1} and the visible laser is tuned in the vicinity of the $\nu_1' = 0 \leftarrow \nu_1'' = 0$ band. We find the $1 \leftarrow 1$ band at $15\,777\text{ cm}^{-1}$, 24 cm^{-1} red shifted from the $0 \leftarrow 0$ band. Figure 5 shows this result, with the IR laser tuned to 2390.9 cm^{-1} (see below).

Once the position of the $\nu_1' = 1 \leftarrow \nu_1'' = 1$ band is known, the antisymmetric stretch frequency in the ground electronic state can be measured in an enhancement experiment by using vibrationally mediated photodissociation. Figure 4 (bottom) shows the vibrational action spectrum obtained by tuning the IR laser and monitoring the fragment ion yield, with the visible laser at the $\nu_1' = 1 \leftarrow \nu_1'' = 1$ electronic transition at $15\,777\text{ cm}^{-1}$. In the enhancement experiment, we monitor the VO^+ fragment, because it is the major product following excitation of $\nu_1' = 1$; excitation of the origin band ($\nu_1' = 0$) primarily produces V^+ . There is some background VO^+ fragment signal due to photodissociation of vibrationally unexcited $V^+(OCO)$, but the fragment yield doubles when the IR laser excites the OCO antisymmetric stretch vibration. This greatly improves the

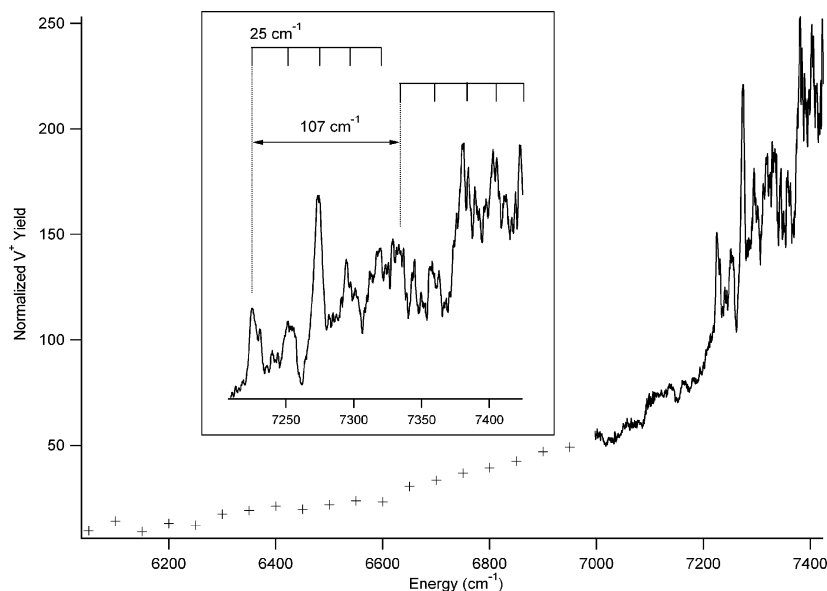


Figure 2. Photodissociation spectrum of $V^+(OCO)$ in the near-IR obtained by monitoring the V^+ fragment. Data at lower energy were obtained by using difference mass spectra (+), due to the low fragmentation yield. At higher energies data were taken at higher resolution, using gated integrators. The inset shows an expanded view of the high-energy portion. Peaks in the spectrum repeat with a 107 cm^{-1} spacing, likely due to combination bands involving the metal–ligand stretch.

TABLE 1: Experimental and Calculated Vibrational Frequencies of $V^+(OCO)$ and CO_2 ^a

$V^+(OCO)$	ν_1 OCO antisym stretch	ν_2 OCO sym stretch	ν_3 $V^+-(OCO)$ stretch	ν_4 OCO bend	ν_5 $V^+-(OCO)$ rock
$^5\Sigma$ ground state (calcd)	2436	1371	242	629	65
$^5\Delta$ ground state (calcd)	2439	1379	264	626	59
ground state (expt)	2392.0		210		
[6.0] state (near-IR) (expt)			107		25
[15.8] state (visible) (expt)	2368		186	597	105

CO_2	ν_1 OCO sym stretch	ν_2 OCO bend	ν_3 OCO antisym stretch
ground state (calcd)	1354	667	2389
ground state (expt)	1333	667.38	2349.16

^a Calculations are at the B3LYP level, with the CEP-121G basis set for V and AUG-cc-pVDZ basis for C and O.

signal-to-noise ratio over the depletion experiment, allowing a much finer scan with the gated integrators. The resolution of the vibrational action spectrum is limited only by the IR laser line width. As a result, the spectrum clearly shows P and R branches, establishing that $V^+(OCO)$ is linear. The simulation assumes a $^5\Sigma$ state and uses $B'' = B' = 0.057\text{ cm}^{-1}$, which is the value given by our density functional theory calculations. Because the rotational constants are so small, the simulated spectrum is not very sensitive to B' or B'' , but $B' - B''$ affects the relative intensities of the P and R branches. The separation between the branches reflects the 12 K rotational temperature of the ions. The simulation gives $\nu_1'' = 2392.0\text{ cm}^{-1}$. The OCO antisymmetric stretch frequency in the excited electronic state is thus $\nu_1' = 2392.0 - 24 = 2368\text{ cm}^{-1}$. This is the first use of vibrationally mediated photodissociation for spectroscopy of an ion.

Discussion

The OCO antisymmetric stretch in $V^+(OCO)$ is blue shifted by 43 cm^{-1} from its value in bare CO_2 . Hybrid density functional theory calculations were carried out to try to predict the vibrational frequencies of $V^+(OCO)$. These calculations use the B3LYP functional, the CEP-121G basis set^{37,38} for V and

the AUG-cc-pVDZ³⁹ basis for C and O and were carried out with Gaussian 03.⁴⁰ Results for CO_2 and $V^+(OCO)$ are summarized in Table 1. The calculations predict that $V^+(OCO)$ is linear, with bond lengths of 2.153 (V–O), 1.181 (O–C), and 1.150 Å (C–O) for the $^5\Sigma$ state and 2.105, 1.183, and 1.149 Å for the $^5\Delta$ state, in good agreement with the study of Sodupe et al.²⁰ Also, calculations show that the $^5\Delta$ state is 0.15 eV lower in energy. The calculations predict that binding to V^+ results in a 47 or 50 cm^{-1} blue shift in the OCO antisymmetric stretch for the $^5\Sigma$ and $^5\Delta$ states, respectively, in excellent agreement with the 43 cm^{-1} shift we observe. Calculations using several other basis sets predict similar shifts. The calculated metal–ligand stretch frequencies are also similar to our observed values.

Because they correlate to $3d^34s$ states of V^+ , the two excited electronic states of $V^+(OCO)$ investigated here are expected to have a longer metal–ligand bond than the ground state. Vibrational peaks in the visible band show partially resolved, red-shaded rotational structure (Figure 5), indicating that the rotational constant decreases (the V^+-O bond length increases) following electronic excitation. A Franck–Condon simulation⁴¹ of the V^+-OCO stretch progression shown in Figure 3 predicts the V^+-OCO bond lengthens by $0.14 \pm 0.02\text{ \AA}$ in the excited state. The increased bond length also reduces the metal–ligand

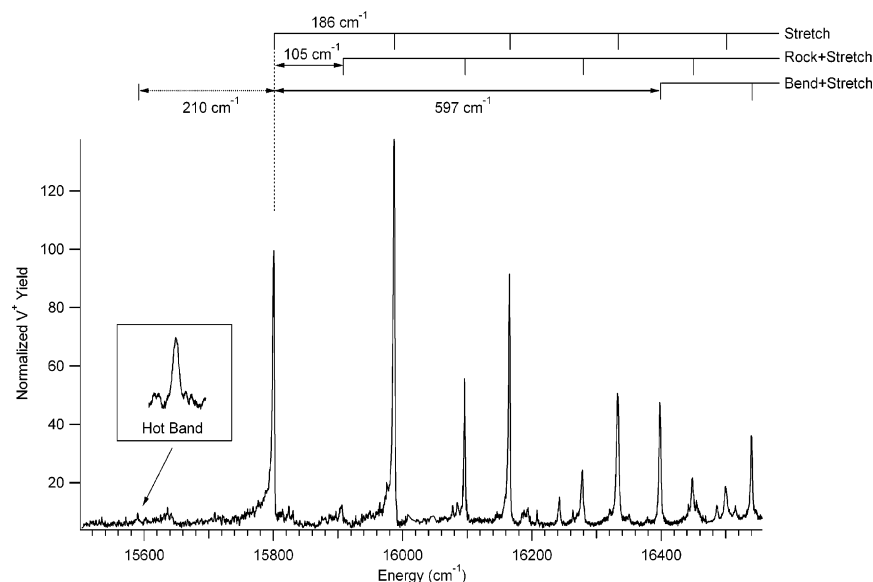


Figure 3. Photodissociation spectrum of $V^+(OCO)$ in the visible region obtained by monitoring the V^+ fragment. The assignment is that of Brucet and co-workers (ref 22) with the origin at $15\,801\text{ cm}^{-1}$, an extended progression in the $V^+(OCO)$ stretching mode at 186 cm^{-1} , and short progressions and combination bands involving the $V^+(OCO)$ rock at 105 cm^{-1} and the OCO bend at 598 cm^{-1} . The inset shows a hot band at $15\,591\text{ cm}^{-1}$ that is shifted by 210 cm^{-1} from the origin peak and is assigned to the V^+OCO stretch in the ground state.

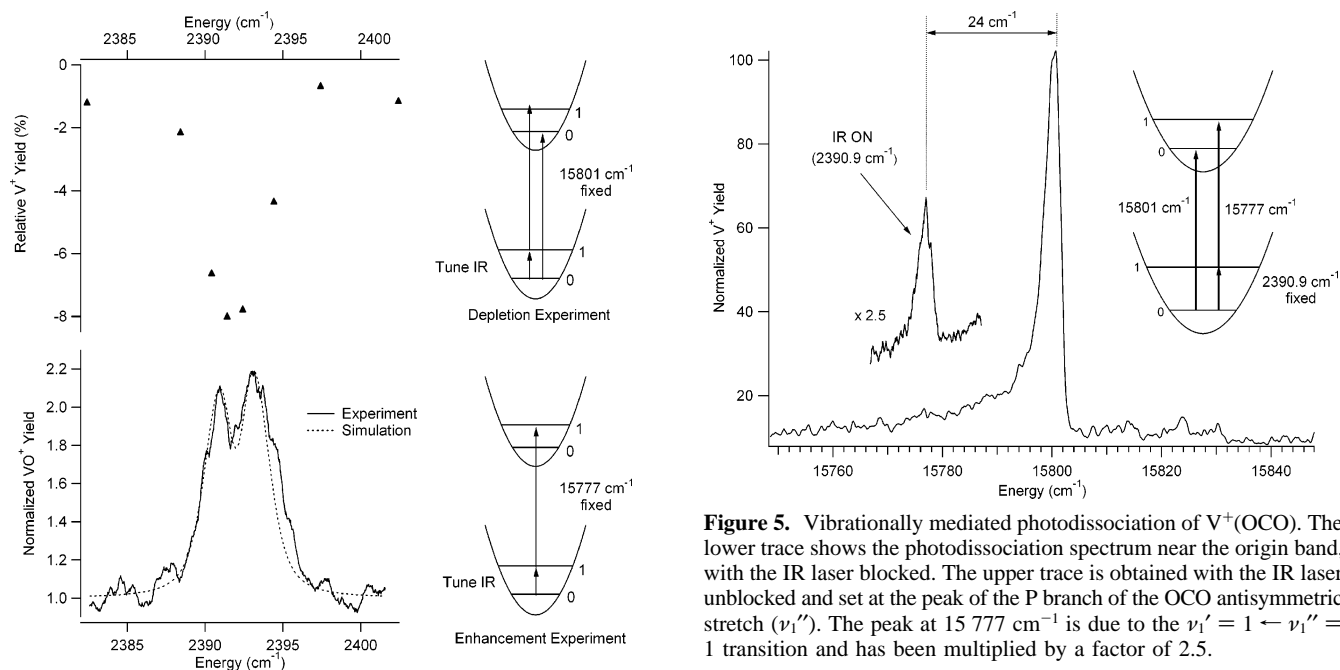


Figure 4. Vibrational action spectra of $V^+(OCO)$ in the OCO antisymmetric stretch region. (Top) Spectrum obtained by monitoring depletion in the V^+ photofragment produced by irradiation at the vibronic origin ($15\,801\text{ cm}^{-1}$). IR absorption near 2391.5 cm^{-1} removes molecules from $v'' = 0$, leading to an 8% reduction in the fragment yield. (Bottom) Spectrum obtained by monitoring enhancement in the VO^+ fragment yield while the IR laser is tuned, with the visible laser fixed at $15\,777\text{ cm}^{-1}$ (the $\nu_1' = 1 \leftarrow \nu_1'' = 1$ transition). The simulated spectrum gives a more precise value of the OCO antisymmetric stretch vibration in $V^+(OCO)$ of 2392.0 cm^{-1} .

stretch frequencies to 107 and 186 cm^{-1} in the excited states, compared to 210 cm^{-1} for the ground state.

Duncan and co-workers have studied vibrational spectroscopy of $V^+(OCO)_n$ ($n \geq 2$) and $V^+(OCO)_nAr$ ($n \geq 1$) in the OCO antisymmetric stretch region using resonance enhanced IR photodissociation.²³ They find that binding to V^+ blue shifts the stretching frequency and attribute this to V^+O repulsion during the vibration. Consistent with this explanation, the blue

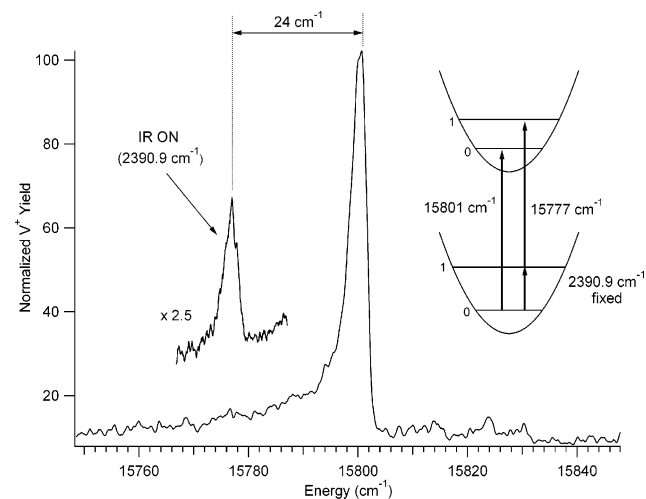


Figure 5. Vibrationally mediated photodissociation of $V^+(OCO)$. The lower trace shows the photodissociation spectrum near the origin band, with the IR laser blocked. The upper trace is obtained with the IR laser unblocked and set at the peak of the P branch of the OCO antisymmetric stretch (ν_1'). The peak at $15\,777\text{ cm}^{-1}$ is due to the $\nu_1' = 1 \leftarrow \nu_1'' = 1$ transition and has been multiplied by a factor of 2.5.

shift becomes smaller for larger clusters, as increased ligation causes the metal–ligand bonds to weaken and lengthen. They observe the same effect in $Fe^+(OCO)_n$ ⁴² and $Mg^+(OCO)_n$.⁴³ Our work supports and extends this observation. They were unable to dissociate $V^+(OCO)$, and $V^+(OCO)Ar$ gives a weak spectrum, with a peak at 2378 cm^{-1} (29 cm^{-1} blue shift). It is not surprising that this is a smaller blue shift than the 43 cm^{-1} that we observe for $V^+(OCO)$, as binding to argon should weaken and lengthen the $V^+(OCO)$ bond for this electrostatic complex. Also, the OCO antisymmetric stretch vibration in the [15.8] state, which has a longer metal–ligand bond than the ground state, is 2368 cm^{-1} , a mere 19 cm^{-1} blue shift from free CO_2 . To investigate how the metal–ligand bond length affects the CO_2 ligand vibrational frequencies, we calculated vibrational frequencies for complexes as a function of the $V^+(OCO)$ bond length. At each $V^+(OCO)$ distance, all other bond lengths were optimized for the linear complex. The shifts in the OCO

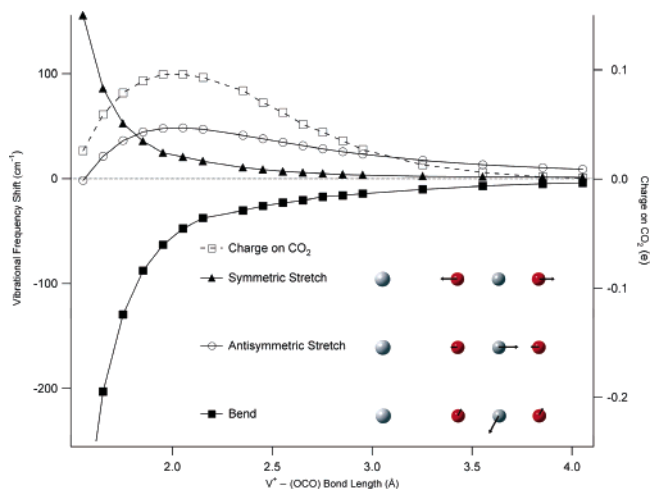


Figure 6. Shifts in CO_2 stretch and bend frequencies in $\text{V}^+(\text{OCO})$ as a function of $\text{V}^+(\text{OCO})$ bond length. The shift in each frequency, relative to the value in bare CO_2 , is shown. Calculations are for the $^5\Sigma$ state at the B3LYP level, using the CEP-121G basis set for V and AUG-cc-pVDZ for C and O. At each $\text{V}^+(\text{OCO})$ bond length, the remaining bond lengths are optimized for the linear complex. The arrows show the vibrational normal modes at the equilibrium geometry. The dashed line shows the charge on the CO_2 ligand, based on a Mulliken population analysis. The shift in the antisymmetric stretch frequency correlates to the charge on the CO_2 .

symmetric, antisymmetric stretch and bend, relative to the values in free CO_2 , are shown in Figure 6. The OCO symmetric stretch frequency increases smoothly and strongly for smaller metal–ligand bond lengths. During the course of this vibration, the $\text{V}^+\text{—O}$ bond length changes significantly, and the frequency shift is clearly due to metal–oxygen repulsion during the vibration. The red shift observed for the bend is likely due to bending motion reducing the $\text{V}^+\text{—O}$ repulsion. The situation for the OCO antisymmetric stretch is more complex. The frequency blue shifts, reaching a maximum near the equilibrium bond length, but it decreases at shorter $\text{V}^+(\text{OCO})$ bond lengths. This is not what would be expected if the blue shift was only due to $\text{V}^+\text{—O}$ repulsion during the vibration. As Figure 6 shows, the OCO antisymmetric stretch almost entirely involves carbon atom motion, with little change in the $\text{V}^+\text{—O}$ bond length. Another factor that may contribute to the observed blue shift is provided by the charge on the CO_2 ligand. Increased CO_2 charge is associated with a higher OCO antisymmetric stretch frequency, as shown in Figure 6.

Conclusions

This study demonstrates that vibrationally mediated photodissociation can be used to measure vibrational frequencies in small, strongly bound molecules. This technique complements infrared multiphoton dissociation and argon tagging and has the potential to measure high-resolution spectra of unperturbed ions, with good sensitivity. More recently, vibrationally mediated photodissociation has also allowed us to investigate how varying the amounts of antisymmetric stretch, metal–ligand stretch, and bend excitation affect the dissociation dynamics of $\text{V}^+(\text{OCO})$.

Acknowledgment. Support for this work by the National Science Foundation (Grant No. CHE-0308439) is gratefully acknowledged.

References and Notes

- (1) Dunbar, R. C. *Int. J. Mass Spectrom.* **2000**, *200*, 571.
- (2) Duncan, M. A. *Int. J. Mass Spectrom.* **2000**, *200*, 545.

- (3) Kleiber, P. D.; Chen, J. *Int. Rev. Phys. Chem.* **1998**, *17*, 1.
- (4) Metz, R. B. *Int. J. Mass Spectrom.* **2004**, *235*, 131.
- (5) Metz, R. B. *Int. Rev. Phys. Chem.* **2004**, *23*, 79.
- (6) Bieske, E. J.; Dopfer, O. *Chem. Rev.* **2000**, *100*, 3963.
- (7) Duncan, M. A. *Int. Rev. Phys. Chem.* **2003**, *22*, 407.
- (8) Lisy, J. M. *Int. Rev. Phys. Chem.* **1997**, *16*, 267.
- (9) Hammer, N. I.; Diken, E. G.; Roscioli, J. R.; Johnson, M. A.; Myshakin, E. M.; Jordan, K. D.; McCoy, A. B.; Huang, X.; Bowman, J. M.; Carter, S. *J. Chem. Phys.* **2005**, *122*.
- (10) Headrick, J. M.; Diken, E. G.; Walters, R. S.; Hammer, N. I.; Christie, R. A.; Cui, J.; Myshakin, E. M.; Duncan, M. A.; Johnson, M. A.; Jordan, K. D. *Science* **2005**, *308*, 1765.
- (11) Okumura, M.; Yeh, L. I.; Meyers, J. D.; Lee, Y. T. *J. Chem. Phys.* **1986**, *85*, 2328.
- (12) Ayotte, P.; Weddle, G. H.; Kim, J.; Johnson, M. A. *J. Am. Chem. Soc.* **1998**, *120*, 12361.
- (13) Crim, F. F. *Annu. Rev. Phys. Chem.* **1993**, *44*, 397.
- (14) Bar, I.; Rosenwaks, S. *Int. Rev. Phys. Chem.* **2001**, *20*, 711.
- (15) Callegari, A.; Rizzo, T. R. *Chem. Soc. Rev.* **2001**, *30*, 214.
- (16) Behr, A. *Carbon Dioxide Activation by Metal Complexes*; VCH Publishers: New York, 1988.
- (17) *Catalytic Activation of Carbon Dioxide*; Ayers, W. M., Ed.; ACS Symp. Ser. 363; Washington, DC, 1988.
- (18) Denise, B.; Cherifi, O.; Bettahar, M. M.; Sneed, R. P. A. *Appl. Catal.* **1989**, *48*, 365.
- (19) Júnior, I. L.; Millet, J.-M. M.; Aouine, M.; Rangel, M. C. *Appl. Catal. A* **2005**, *283*, 91.
- (20) Sodupe, M.; Branchadell, V.; Rosi, M.; Bauschlicher, C. W., Jr. *J. Phys. Chem. A* **1997**, *101*, 7854.
- (21) Sievers, M. R.; Armentrout, P. B. *J. Chem. Phys.* **1995**, *102*, 754.
- (22) Lessen, D. E.; Asher, R. L.; Brucat, P. J. *J. Chem. Phys.* **1991**, *95*, 1414.
- (23) Walker, N. R.; Walters, R. S.; Duncan, M. A. *J. Chem. Phys.* **2004**, *120*, 10037.
- (24) Husband, J.; Aguirre, F.; Ferguson, P.; Metz, R. B. *J. Chem. Phys.* **1999**, *111*, 1433.
- (25) Rothman, L. S.; Jacquemart, D.; Barbe, A.; Benner, D. C.; Birk, M.; Brown, L. R.; Carleer, M. R.; Chackerian, C.; Chance, K.; Coudert, L. H.; Dana, V.; Devi, V. M.; Flaud, J. M.; Gamache, R. R.; Goldman, A.; Hartmann, J. M.; Jucks, K. W.; Maki, A. G.; Mandin, J. Y.; Massie, S. T.; Orphal, J.; Perrin, A.; Rinsland, C. P.; Smith, M. A. H.; Tennyson, J.; Tolchenov, R. N.; Toth, R. A.; Vander Auwera, J.; Varanasi, P.; Wagner, G. *J. Quant. Spectrosc. Radiat. Transfer* **2005**, *96*, 139.
- (26) Gerstenkorn, S.; Luc, P. *Atlas du Spectre D'Absorption de la Molecule D'Iode 14800–20000 cm⁻¹*; Editions du Centre National de la Recherche Scientifique: Paris, France, 1978.
- (27) Sugar, J.; Corliss, C. *J. Phys. Chem. Ref. Data* **1985**, *14*, Suppl. No. 2.
- (28) Hayes, T.; Bellert, D.; Buthelezi, T.; Brucat, P. J. *Chem. Phys. Lett.* **1997**, *264*, 220.
- (29) Hayes, T.; Bellert, D.; Buthelezi, T.; Brucat, P. J. *Chem. Phys. Lett.* **1998**, *287*, 22.
- (30) Lessen, D.; Brucat, P. J. *J. Chem. Phys.* **1989**, *91*, 4522.
- (31) Page, R. H.; Shen, Y. R.; Lee, Y. T. *J. Chem. Phys.* **1988**, *88*, 4621.
- (32) Pribble, R. N.; Zwier, T. S. *Science* **1994**, *265*, 75.
- (33) Brutschy, B. *Chem. Rev.* **2000**, *100*, 3891.
- (34) Ebata, T.; Iwasaki, A.; Mikami, N. *J. Phys. Chem. A* **2000**, *104*, 7974.
- (35) Macleod, N. A.; Simons, J. P. *Phys. Chem. Chem. Phys.* **2003**, *5*, 1123.
- (36) Nir, E.; Hunig, I.; Kleinermanns, K.; de Vries, M. S. *ChemPhysChem* **2004**, *5*, 131.
- (37) Stevens, W. J.; Basch, H.; Krauss, M. *J. Chem. Phys.* **1984**, *81*, 6026.
- (38) Stevens, W. J.; Krauss, M.; Basch, H.; Jasien, P. G. *Can. J. Chem.* **1992**, *70*, 612.
- (39) Woon, D. E.; Dunning, T. H. *J. Chem. Phys.* **1993**, *98*, 1358.
- (40) Frisch, M. J.; Trucks, G. W.; Schlegel, H. B.; Scuseria, G. E.; Robb, M. A.; Cheeseman, J. R.; Montgomery, J. A., Jr.; Vreven, T.; Kudin, K. N.; Burant, J. C.; Millam, J. M.; Iyengar, S. S.; Tomasi, J.; Barone, V.; Mennucci, B.; Cossi, M.; Scalmani, G.; Rega, N.; Petersson, G. A.; Nakatsuji, H.; Hada, M.; Ehara, M.; Toyota, K.; Fukuda, R.; Hasegawa, J.; Ishida, M.; Nakajima, T.; Honda, Y.; Kitao, O.; Nakai, H.; Klene, M.; Li, X.; Knox, J. E.; Hratchian, H. P.; Cross, J. B.; Bakken, V.; Adamo, C.; Jaramillo, J.; Gomperts, R.; Stratmann, R. E.; Yazyev, O.; Austin, A. J.; Cammi, R.; Pomelli, C.; Ochterski, J. W.; Ayala, P. Y.; Morokuma, K.; Voth, G. A.; Salvador, P.; Dannenberg, J. J.; Zakrzewski, V. G.; Dapprich, S.; Daniels, A. D.; Strain, M. C.; Farkas, O.; Malick, D. K.; Rabuck, A. D.; Raghavachari, K.; Foresman, J. B.; Ortiz, J. V.; Cui, Q.; Baboul, A.

G.; Clifford, S.; Cioslowski, J.; Stefanov, B. B.; Liu, G.; Liashenko, A.; Piskorz, P.; Komaromi, I.; Martin, R. L.; Fox, D. J.; Keith, T.; Al-Laham, M. A.; Peng, C. Y.; Nanayakkara, A.; Challacombe, M.; Gill, P. M. W.; Johnson, B.; Chen, W.; Wong, M. W.; Gonzalez, C.; Pople, J. A. *Gaussian 03*, Revision B.03; Gaussian, Inc.: Wallingford, CT, 2004.

- (41) Metz, R. B. *J. Chem. Educ.* **2004**, *81*, 157.
- (42) Gregoire, G.; Velasquez, J.; Duncan, M. A. *Chem. Phys. Lett.* **2001**, *349*, 451.
- (43) Gregoire, G.; Brinkmann, N. R.; van Heijnsbergen, D.; Schaefer, H. F.; Duncan, M. A. *J. Phys. Chem. A* **2003**, *107*, 218.